The nature of trehalose–protein interactions in aqueous solutions revealed by neutron scattering

Nanoscale

PAPER

View Article Online
View Journal | View Issue

Cite this: *Nanoscale*, 2026, **18**, 8609

The nature of trehalose–protein interactions in aqueous solutions revealed by neutron scattering

Kajsa Ahlgren, [a] Christoffer Olsson, [b] Tristan Youngs[c] and Jan Swenson *[a]

Trehalose is widely recognized for stabilising proteins under conditions that promote dehydration, denaturation, or loss of function, yet its underlying mechanisms remain elusive. We examine myoglobin in trehalose solutions of two concentrations to evaluate whether trehalose forms a protective sugar shell beyond the hydration layer—a concept suggested by molecular dynamics simulations but not experimentally verified. Using neutron diffraction, we demonstrate that myoglobin remains almost fully hydrated in both systems, even at high trehalose concentrations. To probe myoglobin–trehalose interactions, we constructed two starting models: (i) trehalose molecules dispersed randomly in the solvent and (ii) a pre-assembled trehalose shell positioned adjacent to the protein surface. After refinement, both models converged with experimental data in the Q range (1–30 Å^{-1}), despite resulting in markedly different final configurations, although the protein was preferentially hydrated by water in both cases. However, the shell model yields substantially higher low-Q intensities (0.03–0.5 Å^{-1}), inconsistent with the experimental data, demonstrating that trehalose does not form a pronounced layer outside the hydration shell. Residue-resolved analysis further confirms that there are almost no direct trehalose–protein interactions for hydrophilic or hydrophobic amino acids. In addition, quasielastic neutron scattering reveals slower dynamics for all components in the concentrated system. Furthermore, the protein motions are considerably slower in the three-component systems compared to those in a trehalose-free binary solution. This finding shows the significance of the dynamically stabilising effect of trehalose on proteins in cryoprotective and pharmaceutical applications.

Received 16th December 2025,
Accepted 23rd February 2026

DOI: 10.1039/d5nr05299h

rsc.li/nanoscale

1 Introduction

Understanding the complex mechanisms by which biological systems maintain their functionality under stress is a fundamental aspect of molecular biology. Central to these mechanisms are the versatile and essential macromolecules, proteins. Their ability to perform an immense number of functions, from catalysing biochemical reactions to providing structural integrity, depends on their appropriate conformation. However, proteins are susceptible to denaturation and loss of function under adverse conditions like dehydration, temperature fluctuations, and freezing.[1] This vulnerability poses significant challenges in biological and biomedical fields, particularly in the preservation of essential biomolecules and organisms.

The stabilising effect disaccharides, especially trehalose, have on proteins has accumulated considerable scientific interest. These sugars have been recognised for their protective qualities and ability to maintain the native state of proteins under stressful conditions.[2–4] Trehalose, in particular, stands out for its efficacy as a cryoprotectant,[5–7] a property crucial in diverse applications ranging from food preservation[8,9] to the safeguarding of human embryos[10] and semen.[11] Despite extensive research, the exact mechanisms by which disaccharides exert this stabilising influence remain elusive. Understanding how the structural and dynamical properties are influenced, the presence of trehalose could enable its utilisation across diverse fields.

There have been many hypotheses with the purpose of explaining the mechanism behind the stabilising effect of trehalose, one of which is the preferential hydration model. The model was first proposed by Arakawa and Timasheff[12] and has since then been reported in many other studies.[13–18] As the name suggests, the theory of the preferential hydration model is that the protein is preferentially hydrated by water molecules. The water molecules surrounding the protein directly interact with the surface of the protein by forming hydrogen bonds with the protein backbone or its side chains.

[a]*Division of Nano-Biophysics, Department of Physics, Chalmers University of Technology, Gothenburg SE-412 96, Sweden. E-mail: jan.swenson@chalmers.se*
[b]*Division of Biomedical Imaging, Department of Biomedical Engineering and Health Systems, KTH Royal Institute of Technology, Stockholm SE-114 28, Sweden*
[c]*ISIS Pulsed Neutron and Muon Source, STFC Rutherford Appleton Laboratory, Didcot, UK*

Meanwhile, the trehalose molecules are preferentially excluded from the protein surface. Previous studies have shown that pronounced preferential hydration is associated with enhanced excluded volume effects, which stabilise the native fold of proteins predominantly through entropic contributions.[19–21] Upon unfolding, proteins expose a larger solvent-accessible surface area, leading to increased exclusion of osmolytes such as trehalose. This exclusion raises the Gibbs free energy of the unfolded state, thereby shifting the equilibrium towards the native conformation and increasing the thermodynamic stability of the protein. While such thermodynamic stabilisation governs protein denaturation and loss of function, the present work focuses instead on dynamic stability, which is governed by solvent-mediated protein dynamics. In particular, the relaxation dynamics of proteins are strongly coupled to the dynamics of hydration water, and a slowdown of hydration water mobility can suppress protein motion,[22,23] leading to reduced activity and ageing processes relevant to applications such as cryopreservation and pharmaceutical protein stabilisation. In a previous study,[24] we analysed the structural properties of a three-component system, consisting of the protein myoglobin (Mb), sugar, and water, by the use of neutron diffraction, which is a commonly used technique to gain insights regarding the structure of a system.[25] We compared the effect of the structurally similar disaccharides trehalose and sucrose. By combining the diffraction data with the empirical potential structure refinement (EPSR) method results,[26] it was shown that the protein is preferentially hydrated by water molecules. Although preferential hydration of Mb was observed in both sugar solutions, it is more pronounced in the case with trehalose.[24] Furthermore, it was observed that the protein–sugar interaction is greater for sucrose compared to that for trehalose, although it is relatively weak for sucrose as well.[24]

Belton and Gil[13] suggested that in systems with low water content, trehalose concentrates the water that is left in the system close to the surface of the protein, enabling hydration of the biomolecule. This has been analysed in a series of molecular dynamics simulation studies[27,28] in which it was observed that the sugar molecules are preferentially excluded from the surface of the protein and that structures involving protein encapsulated in a network of hydrogen bonds between the sugar and the water molecules were formed. In addition, it was suggested by Corradini *et al.*[29] that trehalose forms a "transient cage" surrounding the protein lysozyme, entrapping and reducing water dynamics close to the surface of the protein. However, to the best of our knowledge, this has not been experimentally confirmed. It should be mentioned that the systems we examine in this study are far more diluted compared to the systems in ref. 27–29, which are the systems that this structural model is proposed for.

The hydration layer is of high importance as it enables conformational fluctuations that underlie protein function. The dynamics of a protein is highly dependent on its hydration layer[30] as it enables conformational fluctuations, and it has been proposed that this interfacial water largely governs the protein function.[31] Two types of hydration dependent motions have been described: hydration-shell-coupled motions, which follow the β-relaxation of the hydration water, and solvent-slaved motions, which follow the α-relaxation of the bulk solvent. Both motions are present in bulk, whereas only hydration-shell-coupled motions persist under hydrated solid-state conditions. However, both motions cease to exist under dehydrated conditions. In the aforementioned study,[24] we compared how the dynamics in the system is affected by the presence of trehalose and the structurally similar disaccharide sucrose. We used quasielastic neutron scattering (QENS) to show that the presence of disaccharides reduces water dynamics. This reduction was more pronounced for trehalose than for sucrose: the diffusion constant of water was 7.09×10^{-10} m^2 s^{-1} in the trehalose system, compared with 12.5×10^{-10} m^2 s^{-1} in the sucrose system.[24] The reduced water dynamics, combined with the increased viscosity of the solution, in turn slows down the dynamics of the protein since the motions of the protein are solvent-slaved.[31,32]

Our previous research offered novel perspectives on the distinct behaviours of trehalose and sucrose. However, the relatively high protein concentration in that study limited our ability to investigate whether trehalose can trap water molecules at the protein surface, potentially forming a sugar–water–protein complex, because molecular crowding effects enforce a high proximity of disaccharides and proteins. The system presented in ref. 24, with a protein : sugar : water weight ratio of 1 : 1 : 2, will henceforth be referred to as M25T25W50,† where M, T, and W denote myoglobin, trehalose, and water, respectively.

Myoglobin is a small globular protein composed of 153 amino acids and is commonly used as a model system due to its well-characterized structure and high solubility in water. Although generally considered hydrophilic, there are some regions of myoglobin's surface that are hydrophobic. Out of the 19 different amino acids in myoglobin, phenylalanine (PHE), isoleucine (ILE), leucine (LEU), and valine (VAL) are considered to be hydrophobic due to their nonpolar, aliphatic, or aromatic side chains. Meanwhile, arginine (ARG), lysine (LYS), glutamine (GLU), and aspartic acid (ASP) are considered to have hydrophilic side chains since they include a hydroxyl, amine, or carboxylic functional group. Understanding how trehalose associates with these chemically distinct regions may provide important information about its role in protein stabilization and hydration.

In this study, we have addressed the structural arrangement of trehalose in relation to the hydration layer surrounding the protein myoglobin by the use of neutron diffraction in combination with structural modelling to analyse the possibility of a sugar shell. We have also considered the possibility of trehalose forming hydrogen bonds with specific amino acids based on whether they have a hydrophilic or

† It should be mentioned that the system in ref. 24 also contains a dataset of X-ray diffraction data which is not included in this paper.

hydrophobic side chain. The systems in this study contain both less protein and sugar compared to the system studied in ref. 24, ending up with a protein : sugar : water weight ratio of 1 : 2 : 7; this system will be referred to as M10T20W70. The lower protein and trehalose concentration provides more freedom for both the water and trehalose molecules to self-assemble in any preferred arrangement between the protein molecules. Furthermore, the analysis of the dynamics of the M10T20W70 system was performed using QENS and compared to the previously obtained data of the M25T25W50 system.

2 Methods

2.1 Sample preparation

Fully protonated D-(+)-trehalose (referred to as H-Tre) was purchased from Sigma-Aldrich in its dihydrate form and used without further purification. The deuterated D-(+)-trehalose (referred to as D-Tre) was purchased from Omicron Biochemicals in an anhydrous form where the carbon bound hydrogens had been exchanged for deuterium. Six isotopically different samples were prepared in the same manner as in ref. 18 and 24 but at lower protein and trehalose concentrations. The isotope compositions were as follows:

1. Mb/D-Tre/D_2O (deuteration of exchangeable OH-groups)
2. Mb/H-Tre/D_2O (deuteration of exchangeable OH-groups)
3. Mb/D-Tre/H_2O
4. Mb/H-Tre/H_2O
5. 50–50 mol% mixture of samples 1 and 2
6. 50–50 mol% mixture of samples 1 and 4.

In Sample 3, D-Tre was used as received. In Sample 1, D-Tre was repeatedly dissolved in D_2O followed by drying the solution under vacuum at 70 °C to exchange all hydroxyl hydrogen in trehalose. Lyophilized powdered myoglobin from equine heart was purchased from Sigma-Aldrich and was freeze dried in either D_2O (samples 1 and 2) or H_2O (samples 3 and 4) before use to remove excess water and deuterate the exchangeable hydrogen atoms in the protein (samples 1 and 2).

2.2 Neutron diffraction experiments

All samples were measured inside 1 mm thick $Ti_{0.676}Zr_{0.324}$ containers, which were sealed with a PTFE O-ring and mounted onto an automatic sample changer. The neutron diffraction experiments were performed on the NIMROD instrument[33] at the ISIS Pulsed Neutron and Muon Source, STFC Rutherford Appleton Laboratory, U.K. All measurements were carried out at a temperature of 310 K. The structure factors, $S(Q)$, were obtained from the raw diffraction data using the GUDRUN suite (2015 version).[34] The GUDRUN software package corrects the data for effects such as inelasticity effects, subtracts background and empty can scattering, as well as normalises the scattering to a vanadium standard, as described in more detail in ref. 34. After correction, the function that is used is the total differential scattering cross section

$$S(Q) = \sum_{ij} c_i c_j b_i b_j^* \left(S_{ij}(Q) - 1\right), \quad (1)$$

where Q is the momentum transfer, $c_{i/j}$ and $b_{i/j}$ are the number density and scattering length of atom i or j. $S_{ij}(Q)$ is the partial structure factor of atom types i and j and can be defined as the Fourier transform of the partial pair correlation function, $g_{ij}(r)$. In multi-component systems, $g_{ij}(r)$ describes spatial correlations between atoms of types i and j. The function $g_{ij}(r)$ represents the relative probability density of finding an atom of type j at distance r from atom i, normalised such that $g_{ij}(r) \to 1$ as $r \to \infty$. The partial pair correlation functions are related to the corresponding partial structure factors through[35]

$$S_{ij}(Q) = 1 + 4\pi\rho \int_0^\infty r^2 \left[g_{ij}(r) - 1\right] \frac{\sin(Qr)}{Qr} \mathrm{d}r, \quad (2)$$

where ρ is the average number density.

2.3 Dissolve modelling

Dissolve is a structural refinement method that can be described as an evolved version of EPSR.[36] One main difference is that Dissolve enables the investigation of more complex systems. More information about Dissolve and how it compares to the EPSR method can be found in ref. 36.

The basis of the method is to create a molecular structure of the system that is in quantitative agreement with experimental diffraction data. The species composition of the molecules included in the systems can be found in Table S1 in the SI. The built system is assigned a reference potential, which contains information regarding the bonds, angles, and torsions of the molecules as well as atom charges and Lennard-Jones and Coulomb parameters. The protein structure was obtained from the protein data bank (PDB ID: 1DWR) and the reference potential was based on the OPLS-AA force field.[37] For the water and sugar molecules the SPC/Fw[38] and OPLS-AA[37] force fields, respectively, were used. The Lennard-Jones and Coulomb parameters are listed in Table S2 in the SI. Once the reference potential was assigned and the geometry of the molecules was optimized, the total energy of the system was minimized by performing standard Monte Carlo moves, in the form of translation and rotation of individual molecules, while keeping the internal geometry of the molecules constant.

The model configuration was then compared with the experimental data obtained from the neutron diffraction experiments. The difference between the structure factor ($S(Q)$) of the model and the experimental data is the basis for the empirical potential. The empirical potential was added to the reference potential, which then formed the basis for the new potential. For more details on Dissolve, see ref. 36. This process was repeated until the model no longer improved. Fig. 1 shows the structure factors for the isotopically different samples. The solid lines represent the experimental data while the dashed lines represent the simulated data. The dotted lines are the differences between the experimental and simulated $S(Q)$. Magnified images of the structure factors for the

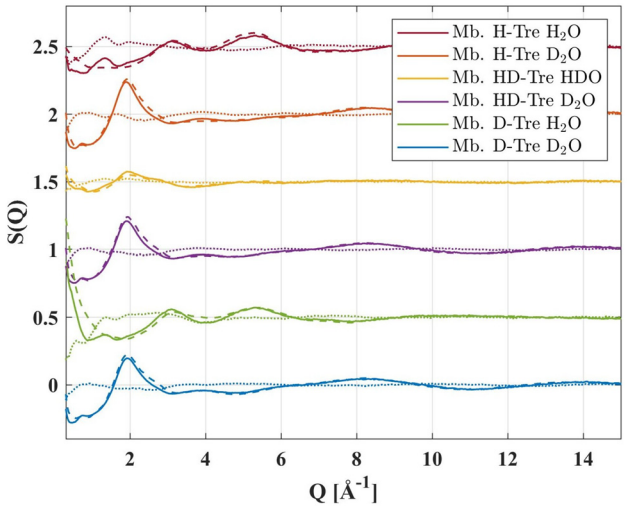

Fig. 1 Structure factor of the six isotopically different samples. The solid lines represent the experimental neutron diffraction data, the dashed lines the Dissolve fits, and the dotted lines the difference between the experimental and simulated curves.

different data sets can be found in Fig. S1–S6 in the SI. As can be seen in these figures the agreement between the experimental and simulated $S(Q)$ is generally good, but some deviations can be observed mainly in the low Q-range of the H_2O containing samples. The reason for these deviations is most likely the difficulty to accurately correct for inelasticity effects for the light hydrogen atoms. The corresponding fits in real-space, $G(r)$, are shown in Fig. S7 in the SI.

After the point where the model could no longer be improved, the simulation was run 1000 iterations more to obtain frames to calculate the pair correlation functions. The pair correlation functions, coordination numbers and hydrogen bonds were calculated using VMD.[39] Three-dimensional representations of the simulation box are shown in Fig. 2, where (a) shows the initial model with randomly distributed molecules and (b) the structurally refined model, with box side lengths l = 103.04 Å. To eliminate potential bias from the randomly oriented and distributed start configuration, an additional model was constructed using a different start configuration. In this alternative model, the trehalose molecules were positioned on a spherical shell with myoglobin placed at the centre. Surrounding the "trehalose-shell", the water molecules were placed on a second shell in order to place them further from the surface of the protein compared to trehalose. Fig. 3 shows the three-dimensional representation of the (a) initial model and (b) after refinement of the spherical trehalose shell model, with box side lengths l = 64.91 Å. This alternative start-configuration will henceforth be referred to as M10T20W70C, where the "C" stands for "clustering". The structure factors, $S(Q)$, of the starting configurations, before potential refinement but after energy minimization, are compared with the experimentally measured $S(Q)$ in Fig. S8 of the SI, where it is evident that the major deviations occur in the low-Q range and that these deviations are substantially larger for the shell model, indicating its inconsistency with the experimental data.

2.4 Quasielastic neutron scattering measurements

All QENS measurements were performed using the IRIS spectrometer[40] at the neutron and muon spallation source ISIS, STFC Rutherford Appleton Laboratory, UK. The following three isotopically different samples were studied at 300 K:

1. Mb/H-Tre/D_2O
2. Mb/D-Tre/H_2O
3. Mb/H-Tre/H_2O

The samples were placed in annular aluminium alloy cans with a sample thickness of 0.1 or 0.25 mm, depending on the

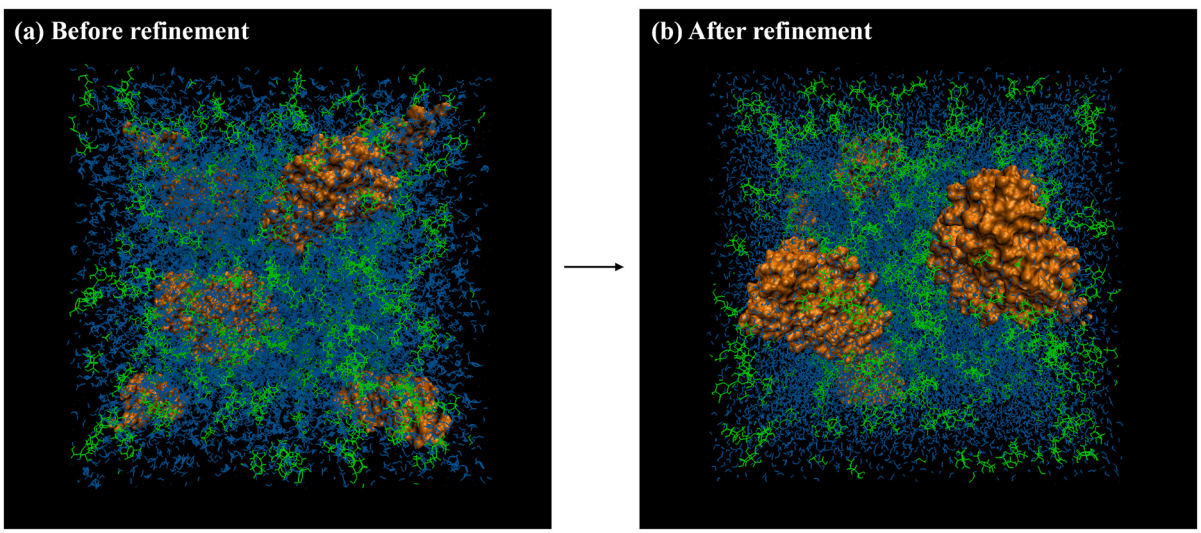

Fig. 2 A three-dimensional representation of (a) the randomly distributed atomistic model (M10T20W70) before and (b) after potential structure refinement. Orange, green and blue represent the protein, trehalose and water, respectively.

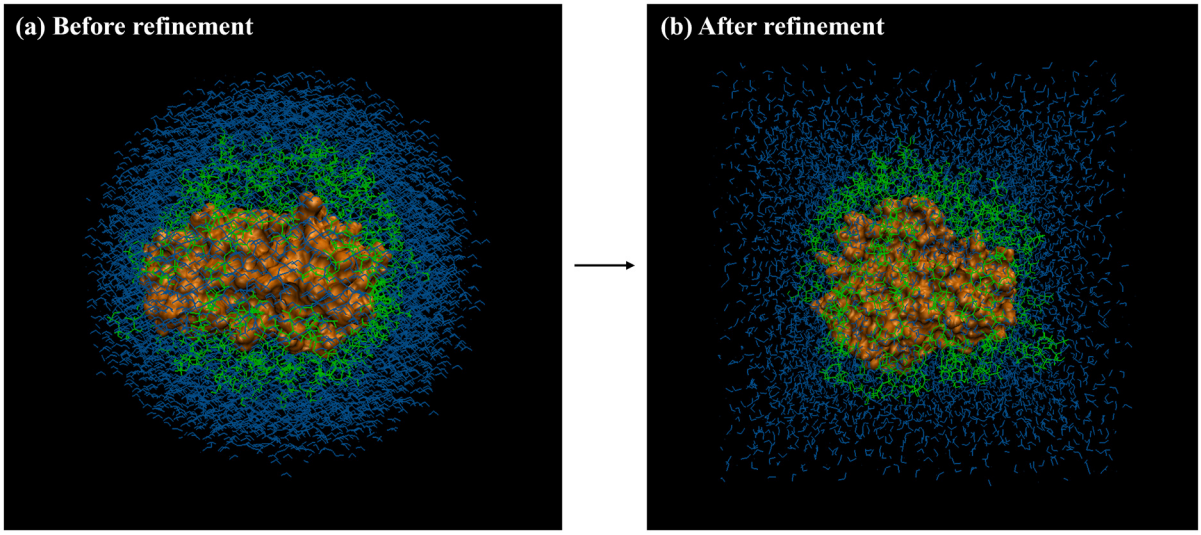

Fig. 3 Three-dimensional representations of the M10T20W70C model. (a) The original configuration before structure refinement contains one protein molecule placed in the centre of the box, surrounded by trehalose on a sphere closest to the surface with water molecules on a second sphere outside the trehalose sphere. (b) The M10T20W70C model after refinement. Orange, green and blue represent the protein, trehalose and water, respectively.

hydrogen content in the sample, to ensure a sample scattering of less than 10%. The PG002 analyser configuration was used, which gave an experimental energy transfer window of ±0.4 meV and an energy resolution of 17.5 μeV at full width at half maximum (FWHM). The spectrometer had 51 detectors, which were grouped into 10 groups with Q-values in the range 0.42–1.8 Å^{-1}.

The dynamic structure factor, $S(Q, w)$, of each sample was obtained by de-convoluting the measured spectra with the resolution function, $R(Q, w)$,[41] which, in turn, was measured by taking the spectra of a vanadium standard. The $S(Q, w)$s were, however, not directly analysed, but Fourier transformed to intermediate scattering functions, $I(Q, t)$, which were used for further analysis. The Mantid software package[41] was used for all data corrections.

2.5 Quasielastic neutron scattering fitting procedure

The dynamics of the three different components in the system are expected to be rather different. Therefore, each experimentally obtained intermediate scattering function, $I(Q, t)$, was fitted by three stretched exponential (KWW) functions using

$$\begin{aligned} I^i(Q,t) = {} & A^i_{\mathrm{Prot}} \exp\left[-(t/\tau_{\mathrm{Prot}})^{\beta_{\mathrm{Prot}}}\right] \\ & + A^i_{\mathrm{Sug}} \exp\left[-(t/\tau_{\mathrm{Sug}})^{\beta_{\mathrm{Sug}}}\right] \\ & + A^i_{\mathrm{Wat}} \exp\left[-(t/\tau_{\mathrm{Wat}})^{\beta_{\mathrm{Wat}}}\right], \end{aligned} \tag{3}$$

where τ represents the relaxation time, $\beta(0 < \beta < 1)$ is the stretching parameter and A^i the amplitude of each relaxation process (which is different for the three isotopically different samples). The A^i of each component in the sample was not a free fit parameter, but rather fixed to its relative contribution to the total scattering cross section of the sample. These amplitudes can be found in Table S3 in the SI. To enable simultaneous fitting of the different $I^i(Q, t)$s, as described in ref. 18, the τ and β of each relaxation process were assumed to be independent of the isotope composition. The average relaxation times were calculated from the obtained fit parameters using

$$\langle\tau\rangle = \frac{\tau}{\beta}\Gamma\left(\frac{1}{\beta}\right), \tag{4}$$

where Γ denotes the gamma function. The Q-dependency of $\langle\tau\rangle$ was fitted using a Gaussian jump-length diffusion model[42]

$$\frac{1}{\tau} = \frac{1}{\tau_{\mathrm{res}}}\left[1 - \exp\left(-\frac{Q^2\langle r^2\rangle}{6}\right)\right], \tag{5}$$

where τ_{res} is the average residence time between two consecutive jumps of the moving atoms‡ and $\langle r^2\rangle$ is the mean square jump-length of these jumps. It should be noted here that this model might be somewhat misleading, in particular for the protein dynamics, where the obtained Q-dependence of the dynamics can equally well be a result of a combination of translational motions (with a Q^2-dependence) and rotational or other local Q-independent motions. However, without knowing the exact nature of the dynamics, the Gaussian jump-length diffusion model gives a reasonable description of the observed Q-dependencies. The diffusion constants were calculated using[42]

$$D_{\mathrm{s}} = \frac{\langle r^2\rangle}{6\tau_{\mathrm{res}}}. \tag{6}$$

‡ Due to the large incoherent scattering cross section of hydrogen, the motions of these atoms are mainly observed.

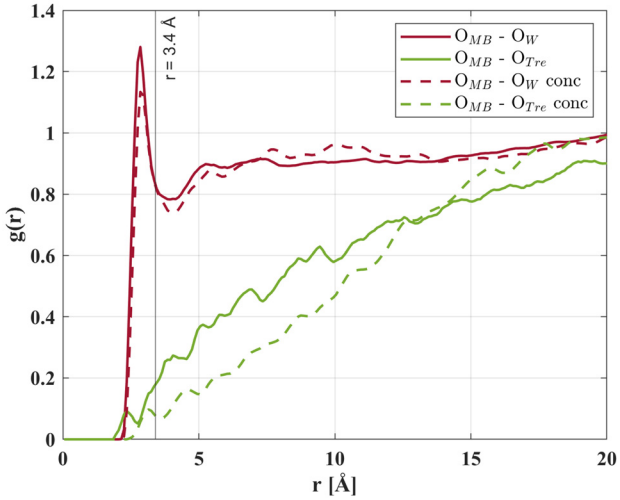

Fig. 4 Partial pair correlation functions between the oxygen atoms on the surface of the protein (O_{MB}) and the oxygen atoms in water (O_W) or trehalose (O_{Tre}). The red solid line represents the correlation between O_{MB} and O_W and the green solid line the correlation between O_{MB} and O_{Tre} in the M10T20W70 system. The corresponding correlations in the M25T25W50 system are presented by dashed lines. The oxygens on the surface of the protein are defined as all O_{MB} within 2.5 Å of any atom of the solvent.

3 Results and discussion

3.1 Structural modelling from neutron diffraction data

The partial pair correlation functions ($g_{ij}(r)$s) between oxygen on the surface of the protein (O_{MB})§ and any oxygen in trehalose (O_{Tre}) or water (O_W) can be seen in Fig. 4. The solid red and green lines represent the O_{MB}–O_W and O_{MB}–O_{Tre} correlations, respectively, for the M10T20W70 system; the dashed lines show the corresponding correlations for the M25T25W50 system. The $g_{ij}(r)$s were calculated from the structural modelling using VMD. For both systems it is shown that the protein is mostly surrounded by water molecules hydrating the protein. In addition, it can be seen that the trehalose molecules are preferentially excluded from the surface of myoglobin and have very little direct interaction with the protein. If trehalose were to form a cage, trapping the water at the protein surface, a peak at around $r \approx 6$ Å would be expected for the O_{MB}–O_{Tre} correlation. This distance from the surface would allow for one layer of water molecules in the hydration layer that separates trehalose from the protein surface. However, as seen in Fig. 4 no peak at that distance can be found, suggesting that trehalose is rather evenly distributed in the area outside the hydrated protein. Moreover, upon formation of a sugar-shell trehalose would be expected to spontaneously form clusters, which has not been observed in previous studies.[43]

§ The oxygens on the surface of the protein are defined as all O_{MB} within 2.5 Å of any atom of the solvent.

From the M10T20W70C system it was observed that the alternative model also converged with experimental data, except in the low Q-range below approximately 1 Å^{-1} (see Fig. S9 in the SI), even though the final structure is quite different from that of the M10T20W70 system. This shows that the experimental data above 1 Å^{-1} are not particularly sensitive to cluster formation or structural inhomogeneities on length-scales above 5 Å. However, it is important to note that also in this model basically all trehalose molecules which initially were located at the protein surface had been replaced by water, *i.e.* the preferential hydration was evident also for this model, which can be seen in Fig. S10 in the SI. In addition, Fig. 5 shows a magnified three-dimensional representation of the M10T20W70C system before (a) and after (b) structure refinement. The orange part is the surface of the protein, and the green and blue stick figures are the trehalose and water molecules, respectively. Before refinement, it can be seen that trehalose is closer to the surface of the protein in relation to the water molecules, whereas after refinement the protein is seen to be preferentially hydrated by water molecules, replacing trehalose at the protein surface. This further strengthens the theory of preferential hydration observed for the M10T20W70 system as well as those in previous studies.[16,18]

A comparison between the experimental and simulated $S(Q)$ for the M10T20W70 and M10T20W70C systems in the low-Q range (Q = 0.03–0.5 Å^{-1}) is presented in Fig. S9–S14 in the SI, where it can be seen that the M10T20W70C system exhibits higher intensities compared to both the experimental data and the randomly distributed model in several datasets. This is because a scattering contrast arises between the trehalose clusters and the rest of the solution as well as the protein. The effect of this depends on the magnitude of the scattering contrast, which should be the largest for samples 2 and 3 (H-Tre in D_2O and D-Tre in H_2O), which is also what we observe from Fig. S11 and S12 in the SI. This indicates that the randomly distributed M10T20W70 model provides a more accurate representation of the atomistic structure of the sample.

Table 1 presents the coordination numbers ($N_{O–O}$) between the oxygen atoms of the first (left) and second (right) molecules. The $N_{O–O}$ was obtained by calculating the average number of a specific pair of atoms that exist within the first coordination shell (0–3.4 Å).

The $N_{O_{MB}–O_W}$ values are 2.39 per surface oxygen in the protein for the M10T20W70 system and 2.06 for the M25T25W50 system. This is reasonable considering that there is more water available in the M10T20W70 system. The $N_{O_{MB}–O_{Tre}}$ values are 0.061 for the M10T20W70 system and 0.042 for the M25T25W50 system. By comparing this to the interaction with water it can be concluded that myoglobin is hydrated by water and that trehalose is not present to a great extent in the first coordination shell for either of the two systems. The difference between $N_{O_{MB}–O_{Tre}}$ in the M10T20W70 and M25T25W50 systems is negligible.

Furthermore, by comparing the $N_{O_{Tre}–O_W}$ and $N_{O_{Tre}–O_{Tre}}$ it can be seen that trehalose is also mainly hydrated by water molecules (2.02 and 0.206, respectively). The low $N_{O_{Tre}–O_{Tre}}$ indicates

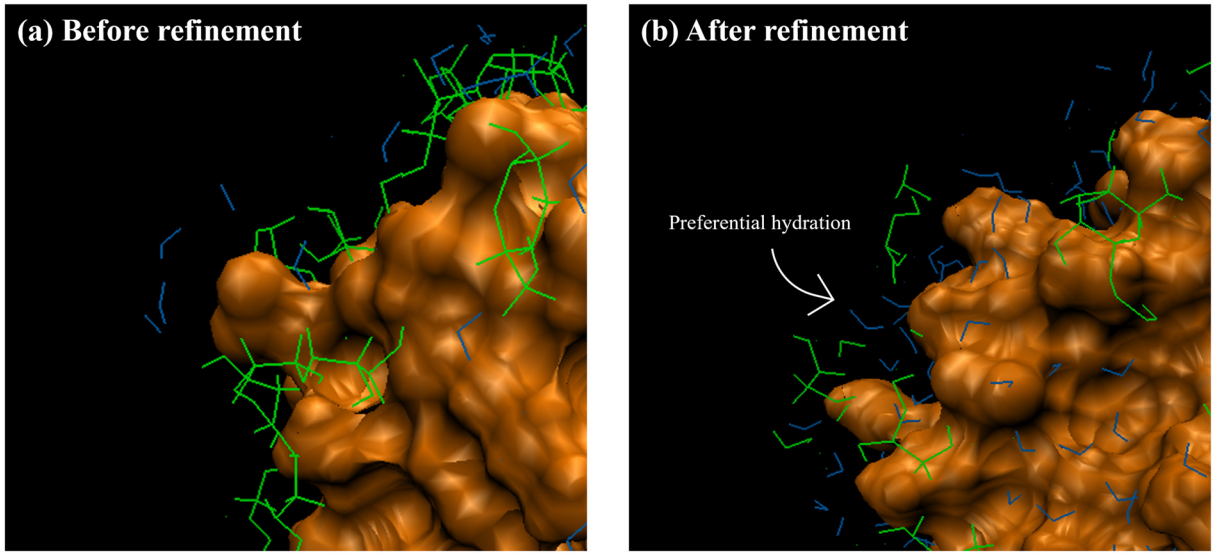

Fig. 5 A magnified three-dimensional representation of the M10T20W70C system (a) before and (b) after refinement. Here only atoms of trehalose or water ≤4 Å from the protein surface are displayed to visualize the first coordination shell. The orange parts represent the surface of the protein, and the green and blue stick figures are the trehalose and water molecules, respectively. Note that only the parts of the trehalose molecules within ≤4 Å of the protein surface are shown.

Table 1 Coordination numbers (N_{O-O}) between oxygens of the first type of molecule and oxygens of the second type of molecule. O–O distances up to r = 3.4 Å are counted. O_{MB} signified the oxygens on the surface of the protein which have been defined as oxygen within 2.5 Å of any atom in the solvent. O_{Tre} denotes any oxygen in trehalose and O_W the oxygen in water. The values without parentheses are for the M10T20W70 system and the values within parentheses are for the M25T25W50 system

	N_{O-O}
O_{MB}–O_W	2.39 (2.06)
O_{MB}–O_{Tre}	0.061 (0.042)
O_{Tre}–O_W	2.02 (1.71)
O_{Tre}–O_{Tre}	0.206 (0.355)
O_W–O_W	4.32 (4.30)

that the trehalose molecules do not cluster to a great extent, which is in agreement with what was shown in ref. 43. If trehalose formed a sugar-shell surrounding the water hydration layer, it would be expected to see a higher $N_{O_{Tre}-O_{Tre}}$ value. If the number given in ref. 18 is calculated per atom, the $N_{O_{Tre}-O_{Tre}}$ would equal 0.355 for the M25T25W50 system, which shows that trehalose clusters less in the more diluted system, which in turn indicates that trehalose is homogeneously distributed in the sample. In Table 1 the $N_{O_W-O_W}$ is 4.32, which is similar to the coordination number observed in ref. 18 ($N_{O_W-O_W}$ = 4.30). A previous study with 33 wt% trehalose and 67 wt% water observed a $N_{O_W-O_W}$ of 4.40,[43] which is slightly higher than that in the present study. Although the trehalose concentration in the system in the present study corresponds to somewhat more hydration (22 wt% trehalose and 78 wt% water), it should be noted that the protein binds a portion of the available water.

The different N_{O-O} correlations discussed above provide information regarding how many oxygen atoms of the second type are located within a certain distance of the oxygen atoms of the first type. However, they do not provide information whether these atoms interact with each other *via* hydrogen bonding or not. By putting an additional restraint on the neighbouring atoms it is possible to calculate the number of hydrogen bonds (HBs) per atom. Since HBs are highly directional, the distance and orientation of the atoms in relation to each other are important. We have chosen the restriction on the distance between the donor (D) and acceptor (A) oxygen (r_{OO}) and the D-hydrogen–A angle (θ_{DHA}) to be $r_{OO} < 3.4$ Å and $\theta_{DHA} \geq 120°$, respectively. The strongest HBs are found when θ_{DHA} is at 170°–180°, which means that weaker HBs are also included here. The total number of HBs between O_{MB} and O_W is 1.17 ± 0.01, which means that almost half of the O_{MB}–O_W atoms within 3.4 Å of each other share a hydrogen atom *via* a HB. The remaining O_W within 3.4 of O_{MB} have a $\theta_{DHA} < 120°$. Interestingly, the number of HBs between O_{MB} and O_W when O_{MB} was chosen as the acceptor was 1.14 ± 0.01, whereas when O_{MB} was chosen as the donor it was only 0.031 ± 0.002. This indicates that the water molecules are more likely to be oriented with the hydrogen atoms closer to the surface of the protein rather than the oxygen atom. This is likely due to the fact that water is a smaller, more mobile molecule, which can easily reorient its hydrogen atoms, compared to the larger and more bulky myoglobin. This is in agreement with the study performed by Qiao *et al.*,[44] where they showed that water molecules within a few Ångströms of the carbonyl groups as well as the negatively charged oxygens at the protein surface were able to orient the hydrogen atoms towards the protein. With water molecules mainly acting as donors, the hydrogen bonds tend

to be stronger, since water's O–H bonds are highly polarized and the molecules are small and flexible in orientation, allowing them to optimize the HB geometry. The total number of HBs between O_{MB} and O_{Tre} is 0.008 ± 0.001, where all have the O_{MB} as the acceptor. Like water, trehalose is more mobile compared to myoglobin which means that the molecule can be oriented more easily. The lack of cases where trehalose acts as an acceptor is likely due to the fact that trehalose would be conformationally restricted with regard to the surface of the protein. This would hinder trehalose from orienting the oxygen atoms close enough while maintaining the angle restriction. Similar results were observed in ref. 43, where it was suggested that water is more likely to act as the HB donor compared to trehalose.

In order to investigate whether trehalose would preferentially orient around certain parts of the protein, rather than forming a "shell", the pair correlation functions between the oxygens in specific hydrophilic or hydrophobic amino acids and O_W and O_{Tre} were analysed. The $g_{ij}(r)$s between oxygens in some hydrophilic amino acids and O_W are shown in Fig. 6(a). Here it can be seen that the correlation between the oxygen in GLU or ASP and the oxygen in water is well pronounced, whereas the same is not seen for LYS and ARG. This is because the side chains of both GLU and ASP contain a carboxylic acid group, which attracts water molecules. The side chain of LYS and ARG contains an amine group and a guanidinium group, respectively. Although these side chains are hydrophilic, they lack an oxygen atom; therefore, the only oxygen available for interaction with water in these amino acids is located in the backbone. Fig. S17 in the SI shows the $g_{ij}(r)$s between any atom in the (a) hydrophilic and (b) hydrophobic amino acids and O_W. There it is shown that the peak at around 2.8 Å is significantly reduced for GLU-O_W and ASP-O_W, suggesting that water mostly interacts with the hydroxyl groups of GLU and ASP. The $g_{ij}(r)$s between any atom in the hydrophobic amino acids and O_W shows a less pronounced interaction compared to that in the hydrophilic amino acids. Fig. S18–S21 in the SI present three-dimensional images from the M10T20W70 model showing that the water molecules are mostly attracted to the side chains of the amino acids rather than the backbone. In Fig. 6(b) it can be seen, as expected, that the correlations between oxygen in the hydrophobic amino acids and water are less pronounced than that in the hydrophilic amino acids. However, a peak can still be observed at 2.8 Å, which can be attributed to the backbone carbonyl group present in ILE, LEU, VAL, and PHE; despite their non-polar side chains, this carbonyl can act as a hydrogen-bond acceptor.

Fig. 7(a) shows the corresponding $g_{ij}(r)$s with O_{TRE}. Here it can be seen that there is little to no direct interaction between the surface of the protein and trehalose. The correlation between ARG and O_{Tre} stands out from those of other hydrophilic amino acids as there are no trehalose oxygens within 6 Å of the oxygen in ARG. One reason for this could be that ARG might have its hydrophilic side chain facing the solvent, which means that the backbone oxygen is further away from trehalose. For hydrophobic amino acids (see Fig. 7(b)) the interaction with trehalose seems to be quite similar to the hydrophilic case: no pronounced interaction can be seen. Fig. S22(a) and (b) in the SI show $g_{ij}(r)$s between any atom in the hydrophilic and hydrophobic amino acids, respectively, and O_{Tre}. Here, no clear interaction pattern can be identified because only very few interactions contribute. Consequently, single interactions generate sharp, isolated peaks that do not reflect the overall characteristics of the system with better statistics.

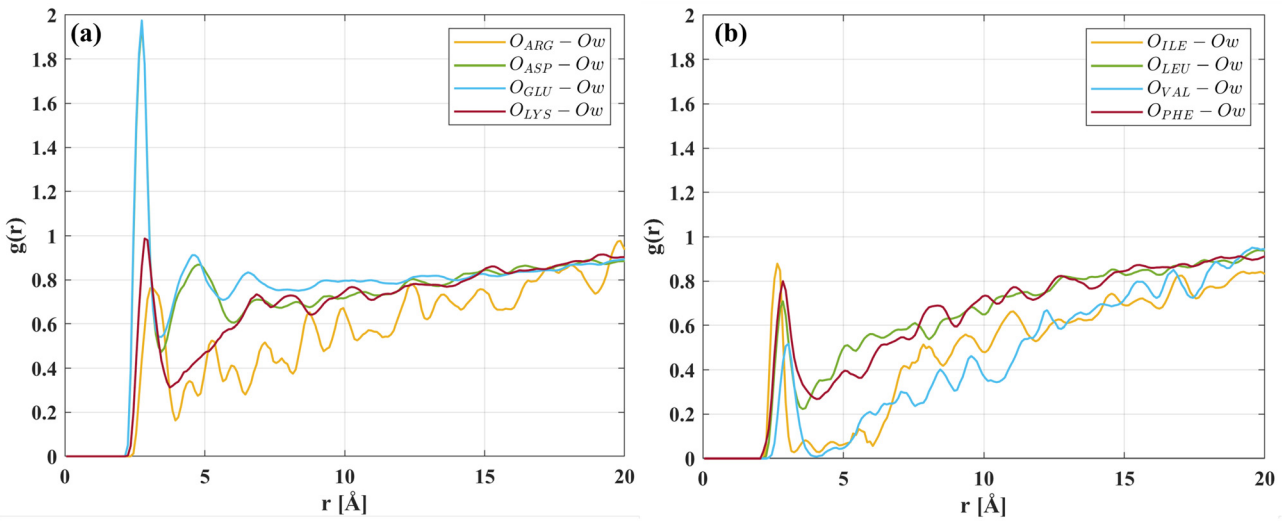

Fig. 6 Partial pair correlation functions between the oxygen atoms on the surface of the protein (O_{MB}) for the hydrophilic (a) and hydrophobic (b) amino acids and the oxygen atoms in water (O_W). The oxygen atoms on the protein surface were defined as those oxygen atoms which are within 2.5 Å of any atom in the solvent.

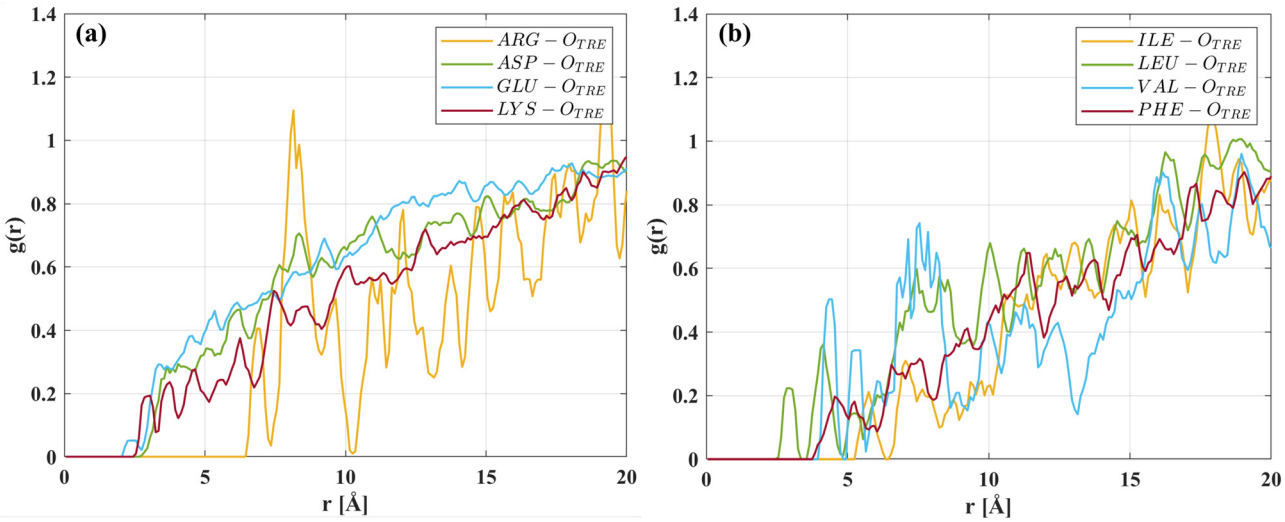

Fig. 7 Partial pair correlation functions between the oxygen atoms on the surface of the protein (O_{MB}) for the hydrophilic (a) and hydrophobic (b) amino acids and the oxygen atoms in trehalose (O_{Tre}). The oxygen atoms on the protein surface were defined as those oxygen atoms which are within 2.5 Å of any atom in the solvent.

3.2 Quasielastic neutron scattering

The dynamics of the different components in the systems were analysed using QENS. The intermediate scattering functions, $I(Q, t)$, at Q = 1.06 Å^{-1} for the M10T20W70 and M25T25W50 systems are shown in Fig. 8(a). To more quantitatively investigate the dynamics of the three different components and how they depend on Q, the experimentally obtained $I(Q, t)$ values were fitted using eqn (3) in the same manner as in ref. 24. The solid lines represent the fits, whereas the markers are the experimentally obtained data. For the Mb/H-Tre/D_2O system the relaxation extends beyond the time window of the experiment for both the M10T20W70 and M25T25W50 systems. Given that the total scattering cross-section of hydrogen is approximately 10 times that of deuterium, this system gives mostly information regarding the dynamics of trehalose and myoglobin. However, it should be mentioned that a significant part of the scattering contribution is attributed to the water due to the diluted conditions of the system. The relative scattering contribution for each component in each sample can be seen in Table S3 in the SI, where it is evident that around 20% of the scattering comes from the water in the M25T25W50 system, and for the corresponding M10T20W70 system water contributes almost 40% to the scattering. Nonetheless, on comparing the protein and trehalose dynamics at the two different concentrations it is evident that they are significantly

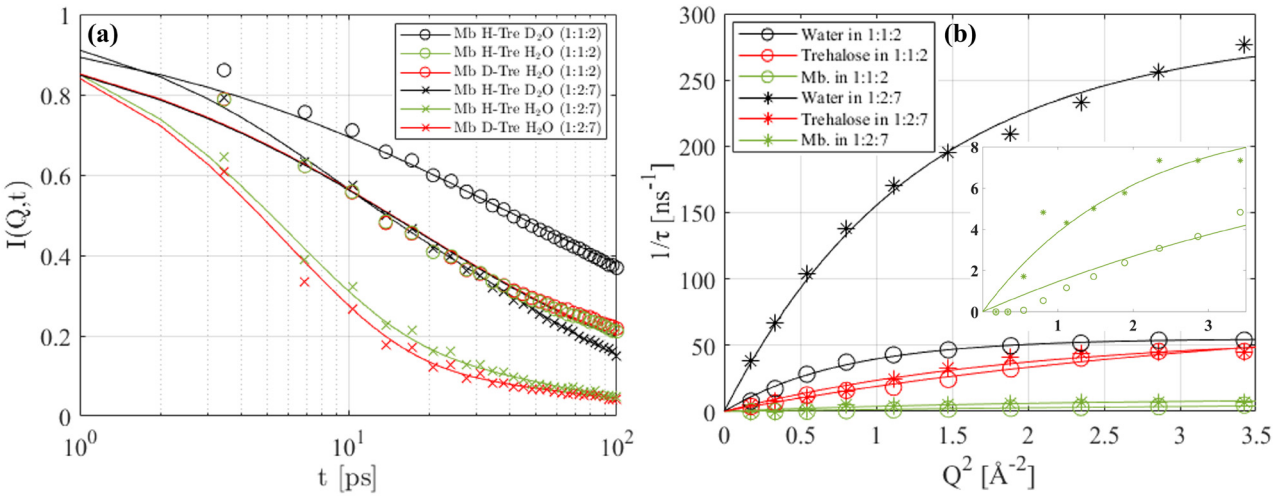

Fig. 8 (a) Intermediate scattering functions as a function of time for both the M10T20W70 and M25T25W50 systems at Q = 1.06 Å^{-1}. (b) Inverse average relaxation times as a function of Q^2. The lines marked with circles represent the M25T25W50 system, whereas the lines marked with stars represent the M10T20W70 system. The inset shows a magnified view of the inverse average relaxation times as a function of Q^2 for Mb.

faster for the M10T20W70 system, as shown in Fig. 8(a). By exchanging D_2O for H_2O it is possible to investigate the dynamics of the water in the system, due to the difference in scattering contributions. Therefore, Mb/H-Tre/H_2O and Mb/D-Tre/H_2O predominantly represent the dynamics of the water in the system and as expected the water in the M10T20W70 system is faster compared to that in the M25T25W50 system. The difference between Mb/H-Tre/H_2O and Mb/D-Tre/H_2O is that the former contains a greater scattering contribution from trehalose, which causes $I(Q, t)$ to decrease slightly slower for the Mb/H-Tre/H_2O system, although they are very similar. In the M25T25W50 system the relaxation of both Mb/H-Tre/H_2O and Mb/D-Tre/H_2O can be seen to extend beyond the time window of the instrument. In contrast, the same systems are almost fully relaxed after 100 ps in the M10T20W70 system, which is partly due to the larger scattering contribution from water and also due to the enhanced dynamics of all three components in the system.

Fig. 8(b) shows the inverse average relaxation time as a function of Q^2. It can be clearly seen that the water dynamics is faster in the M10T20W70 system. The inset shows a magnified image of the inverse average relaxation time for myoglobin in both the M10T20W70 and M2525W50 systems. Here it can be seen that the dynamics of the protein is highly increased by the increased water content.

The average relaxation times at Q = 1.06 Å^{-1} and the diffusion constants of water, trehalose, and myoglobin were calculated using eqn (4) and (6), respectively, and are presented in Table 2. The diffusion constants for trehalose and myoglobin were also calculated using the Gaussian jump-length diffusion model. Since their motions involve a combination of different dynamical processes, a jump-diffusion fit does not represent a literal jump mechanism but yields an effective diffusion coefficient reflecting the averaged motion. The values for the M10T20W70 system are compared with values (within parentheses) for the M25T25W50 system. For the water molecules, the average relaxation time is ~4 times shorter in the M10T20W70 system. Similarly, the average relaxation times for trehalose and myoglobin are ~1.3 and ~3.8 times shorter, respectively, in the more diluted system. As previously mentioned, the M10T20W70 system allows for more water to be available for the hydration of the protein. This not only increases the number of water molecules that can closely interact with the protein, forming a layer of hydration close to the protein surface, but also enhances the dynamics of the protein hydration layer and the surrounding bulk solvent. The water molecules in the hydration shell constantly exchange with the bulk water. This dynamic exchange becomes faster when the average relaxation time decreases and the diffusion constant of the water molecules increases. The enhanced water dynamics is also the reason for the faster dynamics of trehalose and myoglobin in the M10T20W70 system compared to that of the M25T25W50 system. Particularly, the protein dynamics is speeded up to the same degree as that of water since it is slaved by the solvent dynamics.[22,31] Both the water and protein dynamics are approximately a factor of 4 faster in the M10T20W70 system, showing the intimate relationship between the water and protein dynamics, and thereby also the protein function.[22] Many studies have investigated aqueous trehalose solutions and consistently reported that trehalose slows down water dynamics.[7,45–49] In a QENS study, Magazù *et al.*[46] examined 50–50 wt% trehalose–water mixtures at 320 K and found that the diffusion constants of trehalose and water were 0.85×10^{-10} m^2 s^{-1} and 8.31×10^{-10} m^2 s^{-1}, respectively. When compared with the values in Table 2 for the M10T20W70 system ($D_w = 22.5 \times 10^{-10}$ m^2 s^{-1}, $D_{Tre} = 3.03 \times 10^{-10}$ m^2 s^{-1}), it is evident that the dynamics reported in that study are slower, which is expected for the trehalose-richer mixture. In contrast, for the more concentrated M25T25W50 system studied here ($D_w = 7.09 \times 10^{-10}$ m^2 s^{-1} and $D_{Tre} = 2.06 \times 10^{-10}$ m^2 s^{-1}), the water dynamics is slower than that in the work of Magazù *et al.*,[46] whereas the trehalose dynamics is faster. This suggests that the presence of the protein decreases the dynamics of the hydration water and that the dynamics of trehalose is faster due to the more dilute bulk. Furthermore, by the use of MD simulations, Corradini *et al.*[29] found that the dynamics of the water closest to the surface of the protein was reduced to a greater extent in the presence of trehalose. They attributed this effect to the entrapment of the water molecules by trehalose close to the surface of the protein. Molecular dynamics simulations by Vila Verde and Campen[48] further demonstrate that the pronounced rotational slowdown of water in trehalose solutions originates primarily from the topology of the glycosidic linking oxygen and arises from local steric and HB exchange effects acting within sub-nanometer distances of the solute. This suggests that clustering of trehalose would lead to spatially heterogeneous water dynamics, whereas a homogeneous distribution would result in a more uniform slowdown. A similar local mechanistic picture has been reported for protein hydration water, where Sterpone *et al.*[50] showed that slowdown near hydrophobic residues is primarily governed by excluded volume effects, whereas slowdown near hydrophilic sites is additionally influenced by water–protein hydrogen bond strength. Thus, the present results in combination with the results in ref. 29, 46, 48 and 50 show that it is likely that the dynamics of the protein hydration water is slower compared to that of the bulk solvent. By the use of pulsed-gradient-spin-echo nuclear magnetic resonance (NMR), Ekdawi-Sever *et al.*[51] found that the diffusion constant for water and trehalose in aqueous solutions at 303 K

Table 2 Average relaxation times at Q = 1.06 Å^{-1} and diffusion constants (D_x) of the three different components. Values without parentheses represent the M10T20W70 system while the values within parentheses are for the M25T25W50 system. It should be noted here that the diffusion coefficients for the protein are not due to the diffusion of the whole protein molecules, but due to fluctuating motions of amino acids

Component	$\langle\tau\rangle$ (ps)	D_x (10^{-10} m^2 s^{-1})
Water	5.87 (23.3)	22.5 ± 2.30 (7.09 ± 1.09)
Trehalose	40.7 (54.5)	3.03 ± 0.41 (2.06 ± 0.46)
Myoglobin	230 (862)	0.49 ± 0.02 (0.158 ± 0.01)

(22 wt% trehalose) is 13.7×10^{-10} m^2 s^{-1} and 2.79×10^{-10} m^2 s^{-1}, respectively. These values are lower than that for the M10T20W70 system, particularly for water, but this discrepancy is anticipated, as NMR measures the macroscopic long-range diffusion constant over a length scale of a few nanometres, whereas the QENS probe shows more local and therefore faster dynamics on a length scale of typically less than a nanometer. Comparing the average relaxation times of trehalose in the dilute and more concentrated systems shows that the dynamics of the sugar is roughly 1.33 times faster in the dilute case. When this is contrasted with the macroscopic viscosities of the corresponding bulk solutions (1.718 mPa s for the dilute system and 2.81 mPa s for the concentrated system) a roughly similar scaling factor is observed. This parallel provides further support for the finding that trehalose is fairly uniformly distributed throughout the solution rather than forming a sugar shell around the hydration layer of the protein.

From a previous study,[18] the average relaxation time of myoglobin in a system without sugar was calculated to be 188 ps, which is faster than the dynamics of myoglobin in both systems presented here. The composition of the two-component system presented in ref. 18 was 33 wt% myoglobin and 67 wt% water. Comparing this system with the M25T25W50 system highlights the impact of trehalose on the mobility of the protein. Furthermore, our observations extend these insights by showing that the dynamics of myoglobin remains slower in the M10T20W70 system, compared to that of the two-component system presented in ref. 18, despite the significantly higher water to protein ratio. This suggests that while increasing water concentration generally facilitates greater mobility for dissolved molecules due to decreased viscosity and less crowding, the presence of trehalose continues to exert a notable influence on the internal fluctuations in myoglobin. This effect persists despite the increased water content, emphasising the significant role of trehalose in modulating protein dynamics by slowing down the dynamics of both the bulk solvent and the protein hydration water.

Although both the randomly distributed and clustered system converged with experimental data in the higher Q-range, the differences in the lower Q-range indicate that the randomly distributed system is a more accurate representation of the real system. These results suggest that trehalose does not form a sugar shell surrounding the hydration water. Instead, even when initially positioned near the protein surface, trehalose becomes excluded and is replaced by a water hydration layer. Previous studies have shown that the effects of disaccharides on the glass transition temperature and on the denaturation temperature arise from distinct mechanisms.[52] The increase in denaturation temperature and thermodynamic stabilisation of the native state are governed by the solvent structure and preferential hydration effects. In contrast, the glass transition temperature is directly related to protein relaxation dynamics and therefore reflects what we define here as dynamic stability. Our results indicate that trehalose does not bind directly to the protein surface but is preferentially excluded, even in the clustered model. Nevertheless, trehalose slows protein dynamics by slowing down the dynamics of the hydration layer through dynamic coupling between trehalose and hydration water. This observation is consistent with the "slaving" model proposed by Frauenfelder *et al.*,[22] in which protein motions are governed by solvent dynamics. Further support for this interpretation is provided by the QENS data combined with the macroscopic viscosity of the bulk solvent without the protein. Both show a parallel between the change in the average relaxation time of trehalose from the dilute to the concentrated system and the corresponding change in viscosity, suggesting that trehalose is fairly uniformly distributed throughout the sample. However, this does not exclude the possibility that a sugar shell is formed in much more concentrated systems as presented in ref. 27–29.

4 Conclusion

In this study, a three-component system containing myoglobin, trehalose and water was studied by neutron diffraction and structural modelling. Two models with different start configurations, one with trehalose randomly distributed in the solution and another with trehalose forming a shell surrounding the protein, were compared. The results show that after structural refinement trehalose is excluded from the protein surface and myoglobin is preferentially hydrated by water in both models, although a trehalose shell remained outside the hydration layer in the shell-model. Both models converge with experimental data in the Q-range 1–30 Å^{-1}. However, in the low Q-range (0.03–0.5 Å^{-1}) the shell-model is not consistent with experimental data, which excludes that trehalose forms a cage-like shell around myoglobin in the present diluted systems.

Using QENS, we compared the dynamic behaviour of the system under more diluted and more concentrated conditions. As expected, the water dynamics in the M10T20W70 system was significantly enhanced relative to the more concentrated M25T25W50 system. The average relaxation times for both water and myoglobin were approximately 4 times faster in the more diluted system, suggesting a strong coupling between protein and water mobility. Notably, despite the limited structural interaction between trehalose and myoglobin, trehalose still slows down the dynamics of the protein relative to trehalose-free systems. This supports the concept that trehalose influences the motion of proteins indirectly *via* the hydration water. The structural and dynamical insights gained from this study provide further understanding of how trehalose dynamically stabilizes proteins in cryoprotective and pharmaceutical applications.

Author contributions

J. S. designed the project and supervised K. A. and C. O. C. O. prepared all the samples. C. O., T. Y. and

J. S. performed the experiments. K. A. did the analysis of the neutron scattering data and Dissolve modelling. T. Y. developed the Dissolve structure refinement method and supervised its use. The manuscript was written by all authors.

Conflicts of interest

There are no conflicts to declare.

Data availability

The link https://github.com/kajsaahl/DilutedMB includes supplementary information (SI) regarding the modelling using Dissolve. This includes the force field parameters of the OPLS-AA force field that was used for the protein, the pdb-files of the final structures and the input-files used to conduct the Dissolve modelling. The accompanying files are organized as follows. The files "4MB_randomdistribution_20251216" and "TreH2O_sphere_subt_2mod2_EP9_scale2_20251215" are the input files for the M10T20W70 and M10T20W70C systems, respectively. "HEME.itp" contains the force field parameters for the heme group in myoglobin, while "ffbonded.itp", "ffnonbonded.itp", and "topol_Protein_chain_A.itp" contain the force field parameters and topology for the remainder of the protein. "aminoacids.rtp" specifies the atomic charges used for the protein. The files "fixed_heme_4protein_12EP_subtracted_coords11816fixedO.pdb" and "sphere_coords.pdb" contain the three-dimensional structures of the two models.

Supplementary information is available. It includes a description of the model composition for the two systems, along with the Lennard-Jones and Coulomb parameters used for the structure refinement. The theoretical relative scattering contributions for the three different molecules in the isotopically distinct systems are also listed. The SI contains magnified images of the experimental and simulated structure factors for the isotopically different systems, as well as real-space pair correlation functions for both systems. To illustrate differences between the two starting models, structure factors prior to potential refinement are included for both systems. The structure factors and corresponding fits for the M10T20W70C system after potential refinement are also provided, along with a comparison between the two systems and the experimental data in the lower Q range. Finally, partial pair correlation functions and three-dimensional images are included to illustrate correlations between different amino acids and water or trehalose. See DOI: https://doi.org/10.1039/d5nr05299h.

Acknowledgements

We would like to thank Tom Headen for all their help during the neutron diffraction measurements. We also thank Victoria Garcia Sakai for her help with the IRIS experiments. Furthermore, we gratefully acknowledge the Science and Technology Facilities Council (STFC) for access to neutron beam time at ISIS, on the NIMROD diffractometer (RB number: Rb1520094 and Rb1720070) and IRIS (RB number: 1600024). The Dissolve modelling was performed on resources provided by the National Academic Infrastructure for Supercomputing in Sweden using the National Supercomputer Center (NSC) Tetralith cluster through project NAISS2025/5-149. This work was financially supported by the Swedish Research Council (Vetenskapsrådet), grant no. 2019-04020.

References

1 T. Arakawa, S. J. Prestrelski, W. C. Kenney and J. F. Carpenter, *Adv. Drug Delivery Rev.*, 2001, **46**, 307–326.
2 M. Uritani, M. Takai and K. Yoshinaga, *J. Biochem.*, 1995, **117**, 774–779.
3 L. Cordone, M. Ferrand, E. Vitrano and G. Zaccai, *Biophys. J.*, 1999, **76**, 1043–1047.
4 N. K. Jain and I. Roy, *Protein Sci.*, 2008, **18**, 24–36.
5 M. Sola-Penna and J. R. Meyer-Fernandes, *Arch. Biochem. Biophys.*, 1998, **360**, 10–14.
6 J. K. Kaushik and R. Bhat, *J. Biol. Chem.*, 2003, **278**, 26458–26465.
7 S. Magazù, V. Villari, P. Migliardo, G. Maisano, M. Telling and H. Middendorf, *Phys. B*, 2001, **301**, 130–133.
8 A. Patist and H. Zoerb, *Colloids Surf., B*, 2005, **40**, 107–113.
9 D. Kovačević and K. Mastanjević, *Czech J. Food Sci.*, 2011, **29**, 15–23.
10 A. Eroglu, M. Toner and L. T. L. Toth, *Fertil. Steril.*, 2002, **77**, 152–158.
11 M. Schulz, J. Risopatrón, G. Matus, E. Pineda, C. Rojas, V. Isachenko, E. Isachenko and R. Sánchez, *Andrologia*, 2017, **49**, e12757.
12 T. Arakawa and S. N. Timasheff, *Biochemistry*, 1982, **21**, 6536–6544.
13 P. S. Belton and A. M. Gil, *Biopolymers*, 1994, **34**, 957–961.
14 T. Lin and S. N. Timasheff, *Protein Sci.*, 1996, **5**, 372–381.
15 R. D. Lins, C. S. Pereira and P. H. Hünenberger, *Proteins: Struct., Funct., Bioinf.*, 2004, **55**, 177–186.
16 C. Olsson, H. Jansson and J. Swenson, *J. Phys. Chem. B*, 2016, **120**, 4723–4731.
17 S. Ajito, M. Hirai, H. Iwase, N. Shimizu, N. Igarashi and N. Ohta, *Phys. B*, 2018, **551**, 249–255.
18 C. Olsson, S. Genheden, V. García Sakai and J. Swenson, *J. Phys. Chem. B*, 2019, **123**, 3679–3687.
19 A. J. Saunders, P. R. Davis-Searles, D. L. Allen, G. J. Pielak and D. A. Erie, *Biopolymers*, 2000, **53**, 293–307.
20 J. A. Schellman, *Biophys. J.*, 2003, **85**, 108–125.
21 S. Cozzolino, A. Tortorella, P. Del Vecchio and G. Graziano, *Life*, 2021, **11**, 652.
22 H. Frauenfelder, G. Chen, J. Berendzen, P. W. Fenimore, H. Jansson, B. H. McMahon, I. R. Stroe, J. Swenson and R. D. Young, *Proc. Natl. Acad. Sci. U. S. A.*, 2009, **106**, 5129–5134.
23 M.-C. Bellissent-Funel, A. Hassanali, M. Havenith, R. Henchman, P. Pohl, F. Sterpone, D. van der Spoel, Y. Xu and A. E. Garcia, *Chem. Rev.*, 2016, **116**, 7673–7697.

24 K. Ahlgren, C. Olsson, I. Ermilova and J. Swenson, *Phys. Chem. Chem. Phys.*, 2023, **25**, 21215–21226.
25 C. N. Wagner, *J. Non-Cryst. Solids*, 1992, **150**, 1–9.
26 A. K. Soper, *Phys. Rev. B:Condens. Matter Mater. Phys.*, 2005, **72**, 104204.
27 G. Cottone, G. Ciccotti and L. Cordone, *J. Chem. Phys.*, 2002, **117**, 9862–9866.
28 G. Cottone, *J. Phys. Chem. B*, 2007, **111**, 3563–3569.
29 D. Corradini, E. G. Strekalova, H. E. Stanley and P. Gallo, *Sci. Rep.*, 2013, **3**, 1218.
30 J. Swenson, H. Jansson, J. Hedström and R. Bergman, *J. Phys.: Condens. Matter*, 2007, **19**, 205109.
31 P. W. Fenimore, H. Frauenfelder, B. H. McMahon and R. D. Young, *Proc. Natl. Acad. Sci. U. S. A.*, 2004, **101**, 14408–14413.
32 H. Jansson, F. Kargl, F. Fernandez-Alonso and J. Swenson, *J. Chem. Phys.*, 2009, **130**, 205101.
33 D. T. Bowron, A. K. Soper, K. Jones, S. Ansell, S. Birch, J. Norris, L. Perrott, D. Riedel, N. J. Rhodes, S. R. Wakefield, A. Botti, M.-A. Ricci, F. Grazzi and M. Zoppi, *Rev. Sci. Instrum.*, 2010, **81**, 033905.
34 *Disordered Materials XRD*, https://www.isis.stfc.ac.uk/Pages/XRD.aspx.
35 D. S. Sivia, *Elementary scattering theory: for X-ray and neutron users*, Oxford University Press, 2011, pp. 63–92.
36 T. Youngs, *Mol. Phys.*, 2019, **117**, 3464–3477.
37 D. Kony, W. Damm, S. Stoll and W. F. Van Gunsteren, *J. Comput. Chem.*, 2002, **23**, 1416–1429.
38 Y. Wu, H. L. Tepper and G. A. Voth, *J. Chem. Phys.*, 2006, **124**, 024503.
39 W. Humphrey, A. Dalke and K. Schulten, *J. Mol. Graphics*, 1996, **14**, 33–38.
40 C. J. Carlile and M. A. Adams, *Phys. B*, 1992, **182**, 431–440.
41 O. Arnold, J. Bilheux, J. M. Borreguero, A. Buts, S. I. Campbell, L. Chapon, M. Doucet, N. Draper, R. Ferraz Leal, M. A. Gigg, V. E. Lynch, A. Markvardsen, D. J. Mikkelson, R. L. Mikkelson, R. Miller, K. Palmen, P. Parker, G. Passos, T. G. Perring, P. F. Peterson, S. Ren, M. A. Reuter, A. T. Savici, J. W. Taylor, R. J. Taylor, R. Tolchenov, W. Zhou and J. Zikovsky, *Nucl. Instrum. Methods Phys. Res., Sect. A*, 2014, **764**, 156–166.
42 M. Bée, *Quasielastic Neutron Scattering*, Adam Hilger, Bristol, England, 1988, pp. 9–71.
43 C. Olsson, H. Jansson, T. Youngs and J. Swenson, *J. Phys. Chem. B*, 2016, **120**, 12669–12678.
44 B. Qiao, F. Jiménez-Ángeles, T. D. Nguyen and M. Olvera de la Cruz, *Proc. Natl. Acad. Sci. U. S. A.*, 2019, **116**, 19274–19281.
45 S. Magazù, F. Migliardo and M. T. F. Telling, *J. Phys. Chem. B*, 2006, **110**, 1020–1025.
46 S. Magazù, F. Migliardo and M. T. F. Telling, *Eur. Biophys. J.*, 2007, **36**, 163–171.
47 S. Magazù, F. Migliardo and M. Telling, *Food Chem.*, 2008, **106**, 1460–1466.
48 A. Vila Verde and R. K. Campen, *J. Phys. Chem. B*, 2011, **115**, 7069–7084.
49 S. Magazù, F. Migliardo, M. Gonzalez, C. Mondelli, S. Parker and B. Vertessy, *Life*, 2012, **2**, 364–376.
50 F. Sterpone, G. Stirnemann and D. Laage, *J. Am. Chem. Soc.*, 2012, **134**, 4116–4119.
51 N. Ekdawi-Sever, J. J. de Pablo, E. Feick and E. von Meerwall, *J. Phys. Chem. A*, 2003, **107**, 936–943.
52 O. Jonsson, A. Lundell, J. Rosell, S. You, K. Ahlgren and J. Swenson, *J. Phys. Chem. B*, 2024, **128**, 4922–4930.